

PEG cross-linked Chitosan: a biomacromolecule as corrosion inhibitor for sugar industry

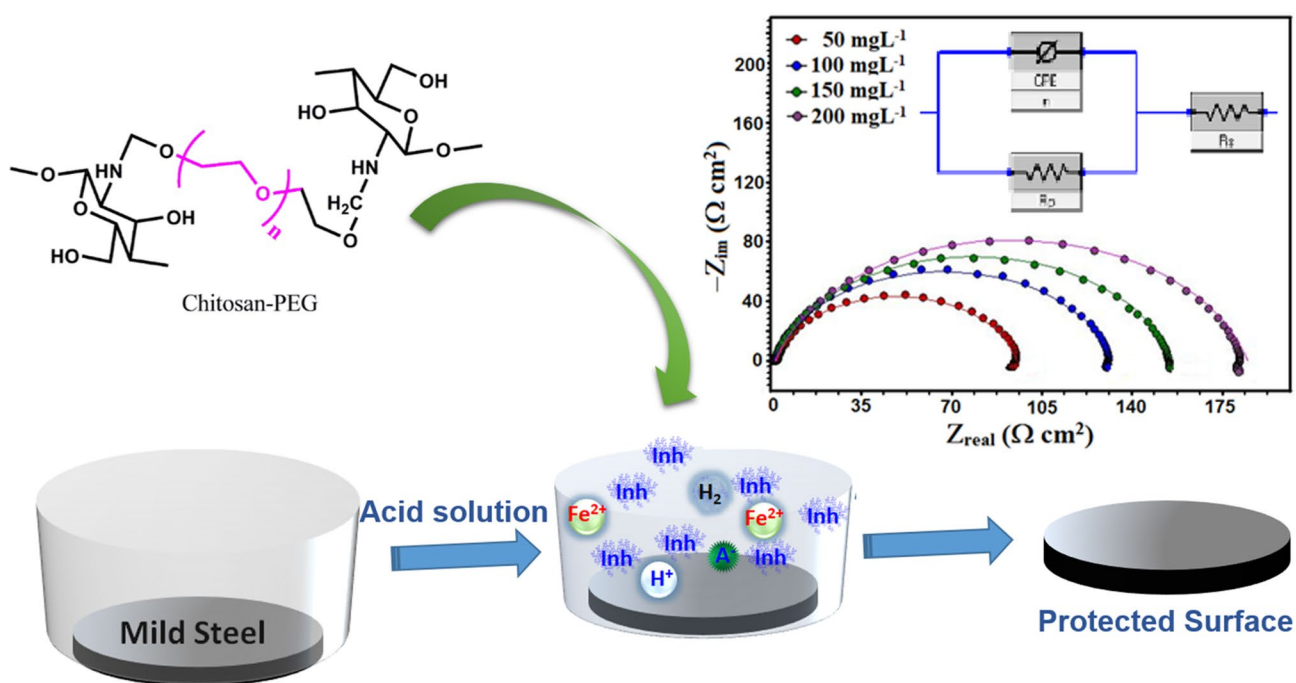
D. S. Chauhan¹ · V. Srivastava² · P. G. Joshi² · M. A. Quraishi¹

Received: 17 April 2018 / Accepted: 18 December 2018 / Published online: 29 December 2018
© The Author(s) 2018

Abstract

The present work reports the application of polyethylene glycol (PEG) cross-linked chitosan (Cht-PEG) as a green corrosion inhibitor. This is the first study reporting the application of Cht-PEG as corrosion inhibitor for mild steel in 1 M sulphamic acid solution. The results of gravimetric measurements, electrochemical study and surface analysis (SEM) are presented in this work. The adsorption of the inhibitor over the mild steel surface obeyed the Langmuir isotherm. At an optimum concentration of 200 ppm, the maximum corrosion inhibition efficiency obtained was 93.9%. The electrochemical impedance spectroscopy (EIS) study showed an increase in polarization resistance with increase in the concentration of inhibitor justifying the adsorption and inhibition behaviour. Potentiodynamic polarization indicated that the Cht-PEG behaved as a mixed type inhibitor with cathodic predominance. The density functional theory (DFT) based calculations supported the experimental observations.

Graphical Abstract



Electronic supplementary material The online version of this article (<https://doi.org/10.1007/s40090-018-0165-0>) contains supplementary material, which is available to authorized users.

Extended author information available on the last page of the article

Keywords Chitosan · Biomacromolecule · Corrosion inhibition · Potentiodynamic polarization · Electrochemical impedance spectroscopy · Density functional theory

Introduction

Sulphamic acid ($\text{H}_2\text{NSO}_3\text{H}$), is used as a cleaning agent in industrial equipment and for the removal of process scales in sugar industry. Sulphamic acid can be used on mild steel and stainless steel without causing pitting or chloride-induced stress corrosion cracking (SCC) [1–3]. The aqueous solutions of sulphamic acid do not emit corrosive fumes but solubilize scales with its $-\text{NH}_2$ and $-\text{OH}$ functional groups thereby forming soluble compounds with most industrial deposits [3–8]. Addition of a corrosion inhibitor to sulphamic acid solution is very important to keep the surface of metal intact and reduce the damage due to corrosion during the cleaning and pickling process. However, most of the synthetic corrosion inhibitors are harmful to the environment, which has directed the attention of scientists on the development of non-toxic green corrosion inhibitors [9, 10].

In this context, the high molecular weight organic polymeric molecules such as carboxymethyl cellulose, Gum Arabic, Tapioca Starch, Chitosan (Cht) and polyethylene glycol (PEG) etc. have been reported as efficient corrosion inhibitors [9–18]. In addition, the PEG cross-linked chitosan hydrogels have been reported for protein and drug release, tissue adhesives and immunotherapy. The introduction of PEG chains to the chitosan matrix improves the solubility and bioavailability of the chitosan-PEG (Cht-PEG) [19–21]. Earlier we have carried out a study on chitosan and its synergism with KI for corrosion inhibition of mild steel in 1 M sulphamic acid and inhibition efficiencies of 73.8% and 90.3% respectively were obtained at 200 mg L^{-1} concentration [15]. We have also reported the application of thiosemicarbazide and thiocarbohydrazide modified chitosan and Schiff bases of chitosan as corrosion inhibitors for mild steel in 1 M HCl [22, 23]. The high efficiency of chemically modified chitosan [24] prompted us to explore the anticorrosion property of PEG modified chitosan.

In the continuation of our work on chitosan based corrosion inhibitors, we herein for the first time, report PEG cross-linked chitosan (Cht-PEG) as a novel eco-friendly corrosion inhibitor for mild steel in 1 M sulphamic acid solution. This modification can improve the solubility and molecular weight of the inhibitor leading to enhanced inhibition behaviour. The study was performed using weight loss method, electrochemical measurements, surface morphology and quantum chemical investigation. The corrosion inhibition property was investigated using gravimetric and electrochemical measurements and surface characterization. Theoretical calculations were carried out to corroborate the experimental results.

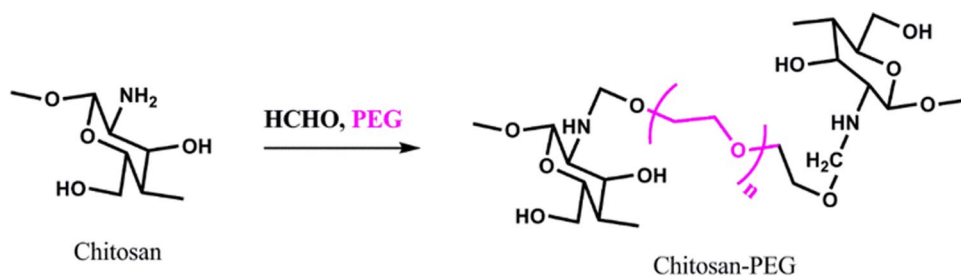
Experimental

Materials and inhibitor synthesis

Polyethylene glycol (PEG; MW 4000) was obtained from SD fine chemicals, Mumbai. Formaldehyde (37% w/w) and formic acid 98–100% were procured from HiMedia, India. All the other chemicals used were of analytical grade and were obtained from Merck India Ltd. Chitosan (MW 50,000 to 190,000 Da; 75–85% deacetylated) was obtained from Aldrich, USA.

The synthesis of PEG cross-linked chitosan (Cht-PEG) was carried out using formaldehyde as reported earlier [25]. Chitosan (1 g) was dissolved in 10 mL formic acid to obtain a viscous solution followed by the addition of 1 g PEG. After stirring for 15 min, 1 mL formaldehyde was added and the solution was mixed thoroughly for 60 min. The resulting Cht-PEG was retrieved by neutralizing with aqueous NaOH. The product so obtained was filtered and washed with water several times followed by drying. The structure of Cht-PEG was characterized using FTIR (Perkin Elmer Version 10.03.05 instrument). A schematic of the synthesis of Cht-PEG is shown in Fig. 1.

Fig. 1 Synthesis of Cht-PEG



Corrosion testing

Gravimetric measurements

The mild steel coupons used for the weight loss and electrochemical measurements had following composition (wt%) C 0.076%, Si 0.026%, Mn 0.192%, P 0.012%, Cr 0.050%, Ni 0.050%, Al 0.023%, Cu 0.135% and balance Fe [9, 10, 26]. The coupons subjected for weight loss study had dimensions of $2.5 \times 2.0 \times 0.025$ cm. After abrading the coupons with SiC paper (grade 600–1200), the samples were rinsed with distilled water, degreased with acetone, dried in hot air, and stored in moisture-free desiccators.

The weight loss studies were carried out following immersion of the mild steel coupons in 1 M sulphamic acid solution in the absence and the presence of varying concentrations of Cht-PEG using the ASTM procedure [27, 28]. After 3 h, the samples were taken out, washed with distilled water and acetone, dried in a moisture free desiccator and again weighed accurately using an analytical balance (precision ± 0.1 mg). The experiments were performed in aerated and unstirred solution at different temperatures.

Electrochemical studies

The electrochemical corrosion testing was performed using a Gamry Potentiostat/Galvanostat (Model G-300) connected with a personal computer with Echem Analyst 5.0 software package [29–31]. The electrochemical cell consisted of a three-electrode assembly where a mild steel strip with an exposed area of 1 cm^2 was used as working electrode, a graphite rod as counter electrode and a saturated calomel electrode (SCE) as reference electrode. Prior to measurements, the working electrode was immersed in the test solution at open circuit potential (OCP) for 30 min to attain a steady state condition. All the electrochemical experiments were performed at 308 K. The electrochemical impedance spectroscopy (EIS) was carried out by an applying AC signal with an amplitude of 10 mV peak to peak at OCP, in the frequency range of 100 kHz to 0.01 Hz [32]. The potentiodynamic polarization measurements were carried out by sweeping the electrode potential automatically from -250 to $+250$ mV vs. OCP at a scan rate of 0.1 mV s^{-1} [29, 31].

Surface analysis

The specimens were immersed in 1 M sulphamic acid solution in the absence and presence of optimum concentration (150 mg L^{-1}) of inhibitor Cht-PEG for 3 h at 308 K. Following the immersion period, the samples were taken out of the test solutions, cleaned with double distilled water and dried. The adsorption of Cht-PEG on the surface of mild steel was studied by performing FTIR in attenuated total reflection (ATR) mode.

The influence of adsorption of inhibitor on mild steel was also studied by recording the surface morphology using scanning electron microscopy (SEM). The SEM images were recorded by a Ziess Evo 50 XVP instrument operating at an accelerating voltage of 20 kV.

Theoretical studies

The quantum chemical calculations were performed on the studied inhibitor using the density functional theory (DFT) method. The DFT calculations were performed using the Becke three-parameter hybrid functional together with the Lee–Yang–Parr correlation functional (B3LYP) and the 6-31+G (d,p) basis set [33, 34]. The calculations were performed using Gaussian 09 software [34, 35] for Windows. The frontier molecular orbital (FOM) energies i.e. the energy of the highest occupied molecular orbital (E_{HOMO}) and the energy of the lowest unoccupied molecular orbital (E_{LUMO}) were evaluated. On the basis of this data, the other parameters were evaluated [9, 10, 26].

Results and discussion

Gravimetric measurements

Effect of inhibitor concentration

The influence of inhibitor concentration (ranging from 50 to 250 mg L^{-1}) on the corrosion inhibition efficiency was studied after 3 h exposure to 1 M sulphamic acid in the absence and presence of Cht-PEG. A graphical presentation of the obtained results is depicted in Fig. 2a. The corrosion rate C_{R} ($\text{mg cm}^{-2} \text{ h}^{-1}$) was computed using Eq. (1) [26, 29, 31]:

$$C_{\text{R}} = \frac{W}{At} \quad (1)$$

where, W denotes the average weight loss of mild steel coupon, A is the total area and t represents the immersion time (3 h). The corrosion inhibition efficiency ($\eta\%$; relative decrease in corrosion rate in the presence of a corrosion inhibitor), was calculated using Eq. (2) [25, 29, 31]:

$$\eta\% = \frac{C_{\text{R}} - C_{\text{Ri}}}{C_{\text{R}}} \times 100 \quad (2)$$

where C_{R} and C_{Ri} are the corrosion rates in the absence and presence of different concentrations of inhibitor, respectively. The surface coverage (θ) was calculated using Eq. (3) [25, 29, 31]:

$$\theta = \frac{C_{\text{R}} - C_{\text{Ri}}}{C_{\text{R}}} \quad (3)$$



Fig. 2 **a** Variation of the inhibition efficiency ($\eta\%$) with inhibitor concentration at 308 K; **b** variation of inhibition efficiency ($\eta\%$) with solution temperature (308–338 K) at optimum concentration of inhibitor; **c** Arrhenius plots of the corrosion rate (C_R) of mild steel in 1 M sulphamic acid in the absence and presence of optimum concentration (200 mg L⁻¹) of Cht-PEG

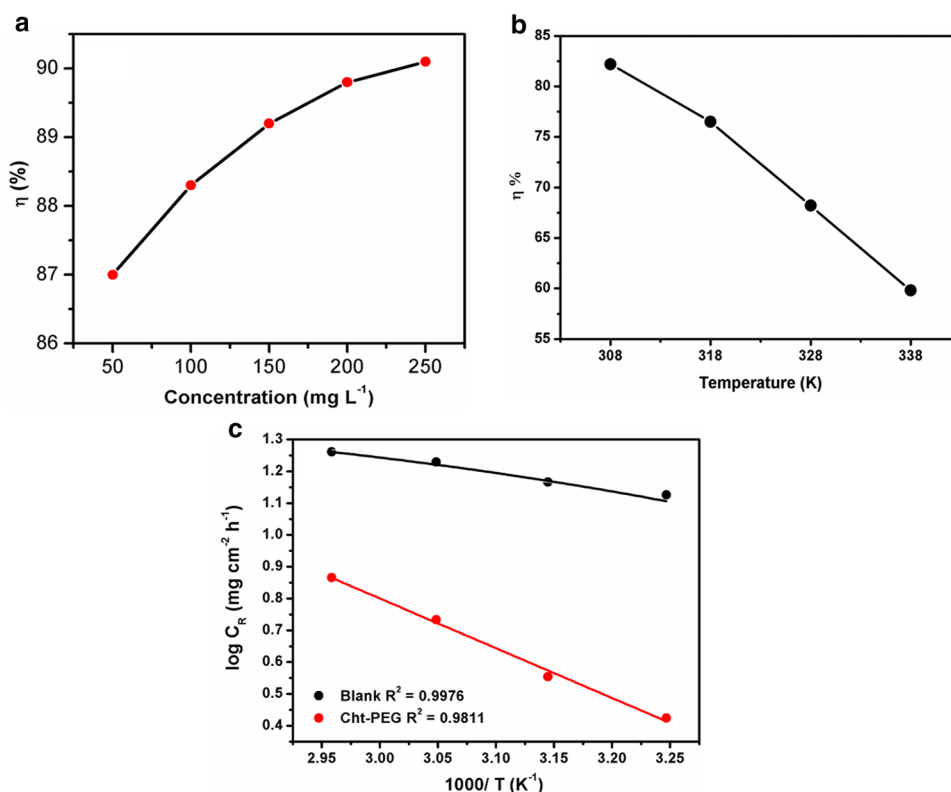


Table 1 Gravimetric parameters obtained for mild steel in 1 M sulphamic acid in the absence and presence of different concentrations of Cht-PEG

	Inhibitor conc. (mg L ⁻¹)	C_R (mg cm ⁻² h ⁻¹)	Surface coverage (θ)	$\eta\%$
Blank	0.0	12.27	–	–
Cht-PEG	50	1.59	0.8704	87.0
	100	1.44	0.8832	88.3
	150	1.32	0.8924	89.2
	200	1.25	0.8993	89.9
	250	1.23	0.9092	90.2

The weight loss parameters viz. corrosion rate (C_R), surface coverage (θ) and the corrosion inhibition efficiency ($\eta\%$) were calculated and presented in Table 1. The increase in inhibition efficiency with increase in concentration of Cht-PEG suggests that the inhibitor acts by adsorbing at the mild steel surface. The inhibition efficiency reached 89.9% at a concentration of 200 mg L⁻¹ beyond which no major increase in $\eta\%$ was observed. Therefore, this concentration was selected as the optimum concentration of the inhibitor for further studies.

Effect of temperature

The influence of temperature on the corrosion inhibition efficiency was studied at the optimum concentration (200 mg L⁻¹) of the inhibitor in the temperature range of 308–338 K. It can be observed from Fig. 2b that the inhibition efficiency decreases with increase in the temperature. A rise in the temperature of the corrosive medium usually accelerates the rates of the corrosion reactions which results in an increased dissolution rate of the metal. An increase in the temperature also leads to an increase in the desorption of the inhibitor molecules from the metal surface which consequently, exposes a greater surface area of the metal sample towards the corrosive attack of the medium and in turns leads to increase in the rate of corrosion [36, 37].

The dependence of corrosion rate on temperature can be elucidated with the Arrhenius equation as given below:

$$C_R = A \exp\left(\frac{-E_a}{RT}\right) \quad (4)$$

where E_a represents the energy of activation, T is the absolute temperature, A denotes the Arrhenius pre-exponential factor and R is the universal gas constant. A plot between $\log C_R$ and $1/T$ is known as an Arrhenius plot which is a straight line with a slope of $E_a/2.303R$ as shown in Fig. 2c. The calculated value of E_a in blank 1 M sulphamic acid was 10.65

kJ mol^{-1} while in the presence of Cht-PEG it was found to be $29.96 \text{ kJ mol}^{-1}$. A higher value of E_a in the presence of inhibitor indicates the creation of a barrier for corrosion process, which raises the activation energy and decreases the rate of metallic corrosion [29, 30]. This observation supports the interaction between the inhibitor molecules and the metal surface [38].

Adsorption isotherm

The adsorption isotherms are used to understand the interaction of inhibitor molecules with metal surfaces. For the adsorption of Cht-PEG over mild steel surface, in the present investigation, several adsorption isotherms were attempted to fit the values of surface coverage θ , among which the Langmuir isotherm provided the best results. The results of other tested isotherms are given in the supplementary information as Fig. S1. The Langmuir isotherm is given by the following equation:

$$\theta/(1 - \theta) = K_{\text{ads}} C \quad (5)$$

where C represents the concentration of the inhibitor and K_{ads} denotes the equilibrium constant for the adsorption process [38]. The curve in Fig. 3 shows a plot of C vs $\log C/\theta$ with the values of the slope and the regression coefficient close to 1. The value of K_{ads} can be calculated from the intercept of the straight line and it was found to be 260.1 L g^{-1} . The K_{ads} is related to the free energy of adsorption $\Delta G_{\text{ads}}^\circ$ according to the following equation:

$$\Delta G_{\text{ads}}^\circ = -RT \ln(1000K_{\text{ads}}) \quad (6)$$

where R is the universal gas constant, T represents the absolute temperature, and 1000 is the concentration of water in g L^{-1} . The value of $\Delta G_{\text{ads}}^\circ$ for Cht-PEG was computed to be $-31.9 \text{ kJ mol}^{-1}$ which suggests that the adsorption of

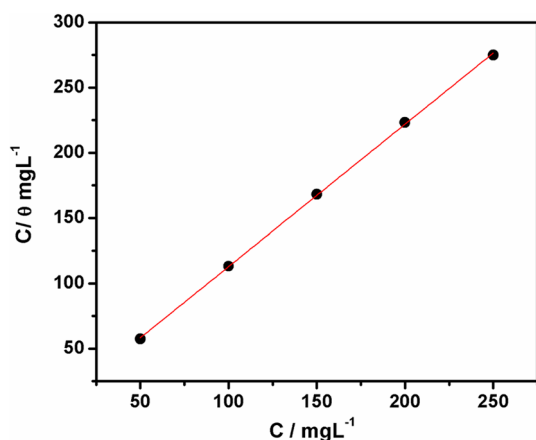


Fig. 3 Langmuir isotherm plot for the adsorption of Cht-PEG on mild steel surface in 1 M sulphamic acid

Cht-PEG follows both physical and chemical modes [29, 31]. The negative sign suggests that the adsorption of Cht-PEG on mild steel surface is a spontaneous process.

Electrochemical studies

Electrochemical Impedance Spectroscopy

The Nyquist plots of the mild steel electrode [39, 42], obtained in 1 M sulphamic acid solution in the absence and presence of different concentrations of inhibitor are shown in Fig. 4. The curves depict depressed semicircles characteristic of a single time constant which shows a charge transfer control of the process. To correctly simulate the electrochemical process taking place at the metal-electrolyte interface, an equivalent circuit model was used as shown in Fig. 4a. The experimental and fitted curves obtained for mild steel in 1 M sulphamic acid in the presence of varying concentrations of Cht-PEG are shown in Fig. 4c. According to the proposed equivalent circuit, the fitted curves exhibit a good agreement with the experimentally obtained impedance data. Here the solution resistance (R_s) represents the collective resistance posed by the solution and the electrical connections. For the blank mild steel solution, the polarization resistance (R_p) contains the charge transfer resistance (R_{ct}) and the double layer resistance (R_d). However, in the presence of the inhibitor, the R_p represents the sum of R_{ct} , the film resistance (R_f) and the resistance R_a (resistance of all accumulated kinds e.g. inhibitor molecules, corrosion products etc.) at the metal-solution interface [40].

In the present study, the constant phase element (CPE) is used in place of the classical double layer capacitor to take into account the depression in the capacitive semicircle which arises due to surface roughness, impurities, dislocations, grain boundaries, adsorbed inhibitor molecules etc. [41]. The CPE represents a frequency distributed double layer capacitance having phase shift (n). By applying the equivalent circuit, the different EIS parameters are evaluated and are shown in Table 2.

The impedance of the CPE is frequency dependent and can be calculated using Eq. (7) [26]:

$$Z_{\text{CPE}} = Y_0^{-1} (j\omega)^{-n} \quad (7)$$

where Z_{CPE} represents the impedance of CPE, Y_0 denotes the magnitude of the CPE (in $\Omega^{-1} \text{ s}^n \text{ cm}^{-2}$), ω is the angular frequency given by $\omega = 2\pi f$ (having units in rad s^{-1}), n is an exponent related to the phase shift and has a value in the range of $0 < n < 1$. The double layer capacitance C_{dl} can be calculated as shown in Eq. (8) [28]:

$$C_{dl} = Y_0 (\omega_{\text{max}})^{n-1} \quad (8)$$

From the data shown in Table 2, it is clear that the successive addition of increasing concentrations of Cht-PEG to



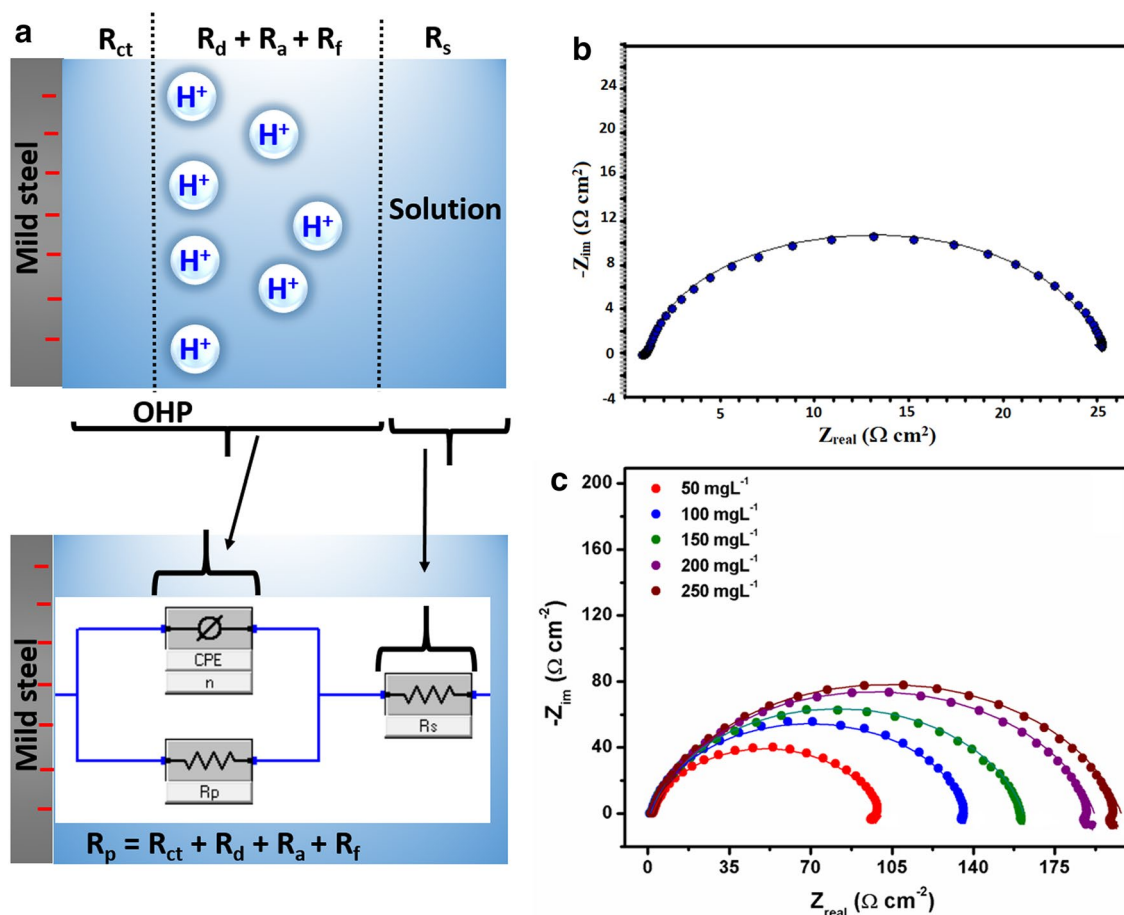


Fig. 4 a Equivalent circuit model used to fit the EIS data; Nyquist plots for mild steel surface in 1 M sulphamic acid in the absence (b) and presence (c) of different concentrations of Cht-PEG at 308 K

Table 2 Electrochemical impedance parameters in the absence and presence of different concentrations of Cht-PEG

	Inhibitor conc. (mg L ⁻¹)	R_s (Ω)	R_p (Ω cm ²)	n	C_{dl} (μF cm ⁻²)	$\eta\%$
Blank		1.03	23.74	0.79	68.7	–
Cht-PEG	50	1.27	93.71	0.83	57.7	76.2
	100	1.52	129.1	0.86	43.9	82.1
	150	1.34	157.3	0.87	36.2	85.3
	200	1.29	192.5	0.89	28.6	88.2
	250	1.31	206.5	0.88	26.6	88.5

the corrosive medium results in an increase in the diameter of the Nyquist semicircles. This shows that the inhibitor molecules get adsorbed on the mild steel surface and block the active sites available for corrosion thereby causing an increase in the R_p values which is attributed to a slower corroding system. The inhibition efficiency can be calculated as given by Eq. (9) [42]:

$$\eta\% = \frac{R_{p(\text{inh})} - R_p}{R_{p(\text{inh})}} \times 100 \quad (9)$$

where $R_{p(\text{inh})}$ and R_p represent the polarization resistance obtained in the absence and presence of inhibitor in 1 M sulphamic acid, respectively. The value of inhibition efficiency ($\eta\%$) increased with increase in the concentration of inhibitor and reached a maximum of 88.2% at 200 mg L⁻¹. However, the values of C_{dl} show a decrease with increase in the concentration. This observation can be explained using the Helmholtz model which relates the double layer capacitance to the thickness of the protective film formed by the inhibitor molecules δ_{org} using following equation [43]:

$$C_{dl} = \frac{\epsilon_0 \epsilon_r}{\delta_{org}} \quad (10)$$

where ϵ_0 and ϵ_r are the permittivity of space and the local dielectric constant respectively. The observed decrease in the C_{dl} values can be attributed to increase in the thickness of δ_{org} with increase in concentration of inhibitor. The decrease in C_{dl} values can also be ascribed to a decrease in the local dielectric constant which suggests that the water molecules with a high dielectric constant are being replaced by the inhibitor molecules having a lower dielectric constant.

Potentiodynamic polarization

Potentiodynamic polarization measurements were performed in 1 M sulphamic acid solution in the absence and presence of varying concentrations of Cht-PEG to evaluate its corrosion inhibition behavior. The representative polarization curves recorded at 308 K are shown in Fig. 5 and suggest that the corrosion current density decreases after addition of the inhibitor to the test solution. The electrochemical

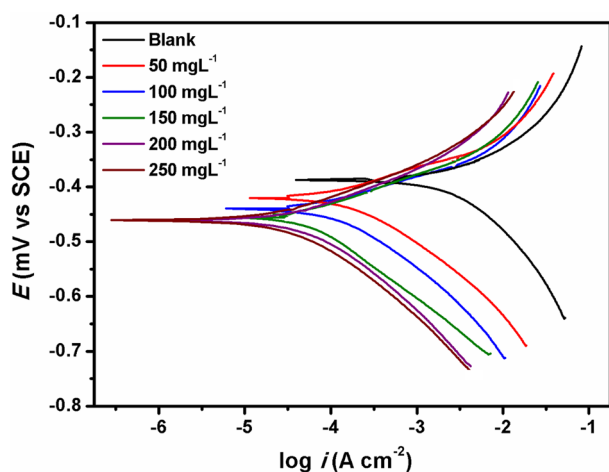


Fig. 5 Potentiodynamic polarization curves for mild steel in the absence and presence of different concentrations of Cht-PEG

Table 3 Potentiodynamic polarization data for mild steel in the absence and presence of different concentrations of Cht-PEG

Inhibitor conc. (ppm)	E_{corr} (mV vs.SCE)	β_a (mV/dec)	$-\beta_c$ (mV/dec)	I_{corr} ($\mu\text{A}/\text{cm}^2$)	$\eta\%$
Blank	-391	77.9	125.4	1697	-
Cht-PEG					
50	-423	73.0	113.3	304.5	82.1
100	-447	69.0	112.7	195.6	88.4
150	-461	68.7	108.6	151.2	91.1
200	-464	63.3	119.7	114.3	93.9
250	-465	61.3	116.7	101.3	94.0

parameters such as the corrosion potential (E_{corr}), corrosion current density (i_{corr}), anodic and cathodic slopes (β_a and β_c) and corrosion inhibition efficiency ($\eta\%$) were calculated from the corresponding Tafel curves and are given in Table 3. The corrosion inhibition efficiency can be calculated from i_{corr} values using following equation [44]:

$$\eta\% = \frac{i_{corr} - i_{corr(inh)}}{i_{corr}} \times 100 \quad (11)$$

where i_{corr} and $i_{corr(inh)}$ are the corrosion current densities obtained for mild steel in 1 M sulphamic in the absence and presence of inhibitor.

It can be observed that the successive addition of increasing concentrations of Cht-PEG results in the reduction of anodic metal dissolution and cathodic hydrogen evolution currents thereby decreasing the corrosion rate. From Table 3, it can be observed that the cathodic Tafel slope (β_c) values are significantly greater than that of the anodic Tafel slope (β_a) values. This indicates that the influence of inhibitor on the kinetics of hydrogen evolution is more prominent than that on the Fe dissolution [28, 29, 43]. In addition, it can be seen that the cathodic polarization curves are almost parallel showing no change in the mechanism of hydrogen evolution. This suggests that the hydrogen evolution process follows a charge transfer mechanism [38]. The inhibitor molecules get adsorbed on the mild steel surface and block the active surface sites available for corrosion reaction. Therefore, the available surface area for hydrogen evolution decreases while the actual mechanism of inhibition remains unaffected. The inhibition behavior becomes more pronounced with increase in the concentration of Cht-PEG. At the optimum concentration of 200 mg L⁻¹, the obtained inhibition efficiency was 93.9% with a little shift in the E_{corr} values towards cathodic side. These results indicate that the Cht-PEG could be classified as a mixed type corrosion inhibitor showing predominantly cathodic influence.



FTIR characterization

The FTIR spectra of Cht and Cht-PEG are shown in Fig. 6a, b respectively. IR (ν max cm^{-1}) 3200 (C–H, sp^2),

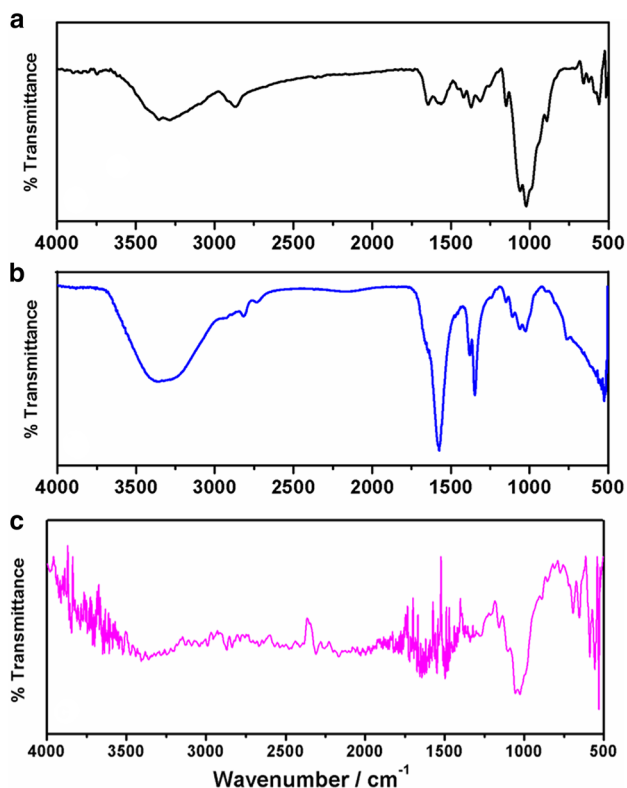


Fig. 6 FTIR spectrum of **a** Chitosan (Cht); **b** Cht-PEG and **c** adsorbed film formed on the mild steel after immersion in 1 M sulphamic acid

1682 (C=O), 1570–1500 (C=C), 1350 (C–N). The Cht-PEG shows the characteristic peaks of Cht along with a new peak appearing at 1280 cm^{-1} due to PEG. The peak at 1580 cm^{-1} appeared with increased intensity due to the amide II band of the cross-linked Chitosan [25]. The FTIR spectrum of mild steel surface recorded in attenuated total reflection (ATR) mode after immersion in 1 M sulphamic acid solution containing optimum concentration of Cht-PEG is shown in Fig. 6c. The spectrum shows the presence of the characteristic peaks from Cht-PEG in the adsorbed film on the metal surface. However, there is a decrease in the intensity and shift in the peak positions which suggests the adsorption of Cht-PEG over mild steel surface [45–48].

Surface morphology

The scanning electron microscopy (SEM) images of the cleaned and abraded mild steel surface in 1 M sulphamic acid in the absence and the presence of optimum concentration of Cht-PEG are shown in Fig. 7a, b, respectively. The image of the blank mild steel sample (i.e., in the absence of inhibitor) depicts considerable damage and surface inhomogeneity due to corrosive attack of the acid solution. The surface morphology of the mild sample in the presence of optimum concentration of Cht-PEG reveals contrasting characteristics. A considerable improvement in the surface smoothness can be easily observed. This is attributable to the adsorption of Cht-PEG over mild steel surface and the formation of a protective film which isolates the mild steel surface from the surrounding corrosive environment. A schematic representation of adsorption

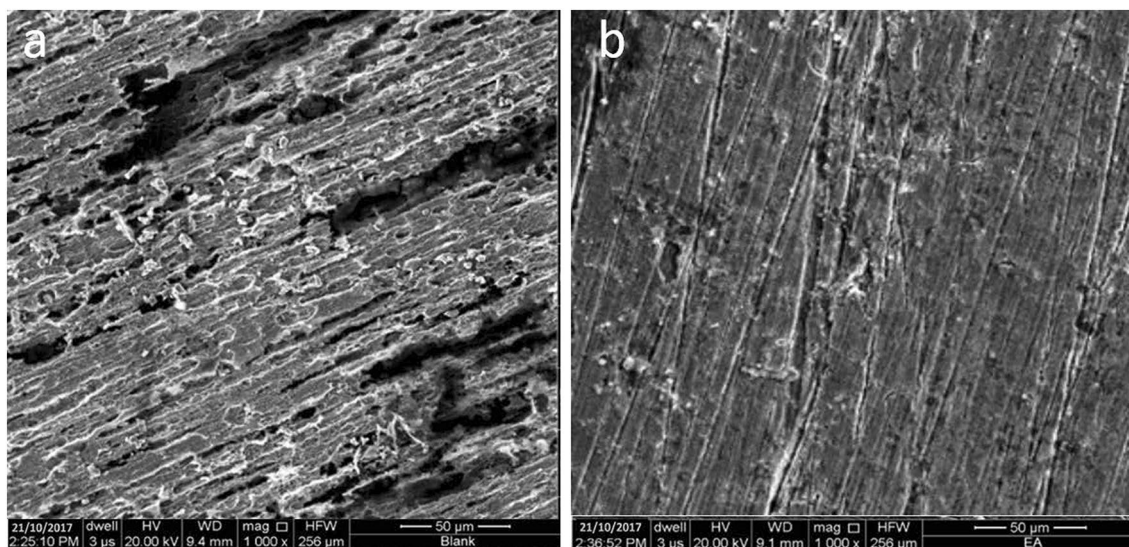
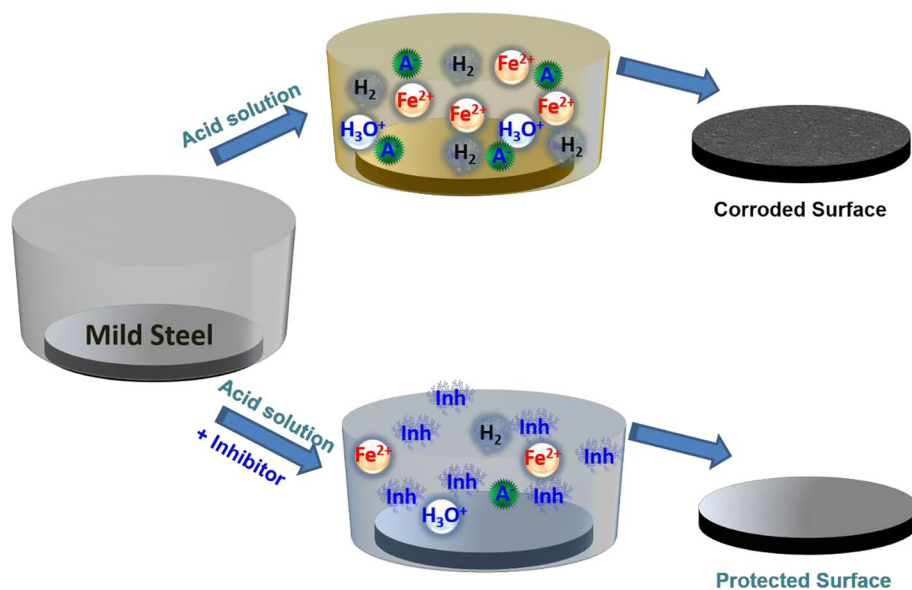


Fig. 7 SEM images of mild steel surface after immersion in **a** 1 M sulphamic acid; **b** in 1 M sulphamic acid containing 200 mg L^{-1} of Cht-PEG

Fig. 8 Schematic representation of corrosion and inhibition behavior of the inhibitor (Cht-PEG) on mild steel surface



and inhibition behavior of the inhibitor (Cht-PEG) on mild steel surface is shown in Fig. 8.

Computational studies

Quantum chemical parameters for metal-inhibitor interaction

Computer-based theoretical methods are frequently employed for predicting structure-activity relationships of pharmaceutically active compounds in the area of corrosion inhibition studies. The density functional theory (DFT) calculations are performed to obtain theoretical parameters such as charge distribution, dipole moment and frontier orbital electron density for designing novel and efficient corrosion inhibitors [49–51]. In the present study, the quantum chemical calculations were performed using density functional theory (DFT) to understand the interaction between inhibitor and the metal surface. In the present study, we performed the calculations on three ethylene glycol units linked between two chitosan units (Cht-EtG) as given in Fig. 9 to understand the effect of functionalization of Cht. The energy of the frontier molecular orbitals (FMO) is important to characterize the electron donation and acceptance tendency of an organic inhibitor. A high value of the energy of the highest occupied molecular orbital (E_{HOMO}) is indicative of the higher tendency of electron donation and a lower value of the energy of the lowest unoccupied molecular orbital (E_{LUMO}) presents a tendency towards electron acceptance. According to HSAB principle, the E_{HOMO} is directly related to ionization potential of a molecule and denotes susceptibility of a molecule towards electrophilic attack. The E_{LUMO} value is related to electron affinity and characterizes the susceptibility of

a molecule towards nucleophilic attack. Frontier molecular orbital theory of chemical reactivity states that the formation of a transition state takes place as a result of an interaction between the frontier orbitals (HOMO and LUMO) of reacting species. Smaller the orbital energy gap between the interacting HOMO and LUMO of molecules, the stronger are the interactions between the molecules of the two reacting species.

In aqueous acidic media, the corrosion inhibitor molecules show the tendency to undergo protonation using the lone pair electrons present on the heteroatoms. Therefore, it is important to understand the reactivity of these protonated species because protonated molecules can also take part in the adsorption process. The preferable site for protonation can be estimated by comparing the proton affinity (PA) values at the different sites [52]. Generally, the heteroatoms of an inhibitor molecule having the most negative Mulliken charges (Table 4) are considered the most probable sites for adsorption. In the present study, the heteroatoms of chitosan i.e., the O33, O35 of the terminal –OH groups; the O8, O31 of the –OH groups adjacent to chitosan ring, the O9, O29 of the terminal –O– groups, the O5, O25 of the chitosan ring –O– groups, the O13 and O19 of the –O– groups from EG units adjacent to chitosan rings, the –O– group present in the center of EG and the N11, N21 of the –NH– groups were considered susceptible for protonation [53]. The proton affinity can be calculated as [54, 55]:

$$PA = E_{\text{proto}} - (E_{\text{non-proto}} + E_{\text{H}^+}) \quad (12)$$

where $E_{\text{non-proto}}$ and E_{proto} are the energies of the non-protonated and protonated inhibitors, respectively. E_{H^+} is the energy of H^+ ion which can be expressed as [56]:

$$E_{\text{H}^+} = E_{(\text{H}_3\text{O}^+)} - E_{(\text{H}_2\text{O})} \quad (13)$$



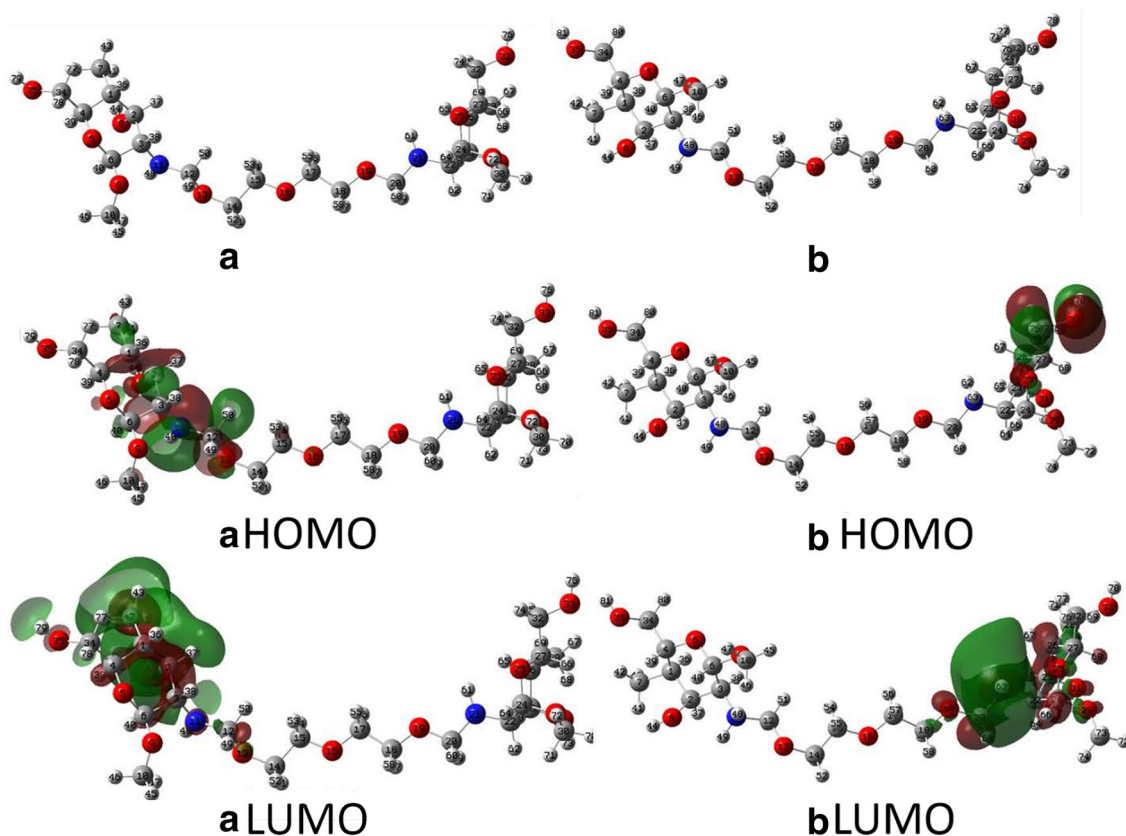


Fig. 9 Optimized structures and frontier orbital electron density distribution (HOMO and LUMO) of **a** Cht-EG neutral and **b** Cht-EG protonated

Table 4 Mulliken charges on heteroatoms of Cht-EG

Heteroatom	Mulliken charge
O5	− 0.530875
O8	− 0.564390
O9	− 0.497101
N11	− 0.559576
O13	− 0.511556
O16	− 0.513348
O19	− 0.520670
N21	− 0.558425
O25	− 0.532869
O29	− 0.475880
O31	− 0.545444
O33	− 0.551656
O35	− 0.554711

where, $E_{(H_2O)}$ is the total energy of a water molecule and $E_{(H_3O^+)}$ is the total energy of the hydronium ion. The PA values at different positions of protonation are listed in Table 5. It can be observed that the preferred sites for protonation are N11, N21 in the Cht-EG structure [45].

Table 5 Proton affinity values at the different positions of Cht-EG

Heteroatoms	PA (kcal mol ^{−1})
O33, O35	− 1130903.31
O8, O31	− 1130886.07
O9, O29	− 1130866.21
O5, O25	− 1130898.15
O13, O19	− 1130888.4
O16	− 1130734.06
N11, N21	− 1130997.31

Following Koopman's theorem, the molecular orbital energies of the FMO can be related to the ionization potential and electron affinity as follows [22, 57–61]:

$$-E_{\text{HOMO}} = I \quad (14)$$

$$-E_{\text{LUMO}} = A \quad (15)$$

where I and A represent the ionization potential and the electron affinity, respectively. The electronegativity and hardness can be computed from the above parameters as shown below:

$$\chi = \frac{1}{2}(I + A) \quad (16)$$

$$\eta = \frac{1}{2}(I - A) = \frac{1}{\sigma} \quad (17)$$

Where, χ represents the absolute electronegativity, η denotes the chemical hardness and σ is the global softness which is the reciprocal of hardness. Hardness can also be related to the molecular orbital energy gap ΔE between HOMO and LUMO. This relation is grounded on the principle of maximum hardness which states that “a molecule arranges itself so as to be as hard as possible” [52, 58, 59]. The electrophilicity index ω and its inverse, the nucleophilicity ϵ can be expressed as:

$$\omega = \frac{\chi^2}{4\eta} = \frac{1}{\epsilon} \quad (18)$$

The fraction of electrons transferred (ΔN) can be given as [22, 49, 55, 56]:

$$\Delta N = \frac{\phi_{Fe} - \chi_{inh}}{2\eta_{inh}} \quad (19)$$

where ϕ_{Fe} represents the work function of the Fe (110) plane having a value of 4.82 eV and the other symbols are as defined above. Accordingly, the calculated quantum chemical parameters for neutral and protonated Cht-EG are listed in Table 6. It can be seen that following protonation, the Cht-EG molecule shows a significant decrease in the E_{HOMO} value compared to that of the protonated molecule indicating a decrease in the tendency to donate electrons. The E_{LUMO} value of the protonated inhibitor also shows a significant decrease indicating an increased tendency of electron acceptance compared to the neutral molecule. Further, after protonation, there is a significant rise in the global electronegativity of the Cht-EG molecule combined together with increased value of the electrophilicity index and the decreased value of nucleophilicity. It can also be observed that while ΔN for neutral inhibitor is 0.46, ΔN for the protonated form is -0.49 . This again suggests that the neutral form of Cht-EG has a tendency to donate the electrons to the metal surface while after protonation the inhibitor molecules exhibit an electron accepting tendency [22, 52, 58]. These parameters further support the increase in electron acceptance tendency compared to that of the electron donation tendency which is exhibited by the neutral Cht-EG molecule.

Table 6 Quantum chemical parameters of the neutral and protonated Cht-EG

Cht-EtG	E_{HOMO}	E_{LUMO}	ΔE	χ	η	σ	ω	ϵ	ΔN
Neutral	-5.0923	1.6699	6.76	1.71	3.38	0.29	0.22	4.62	0.46
Protonated	-10.7352	-4.7457	5.99	7.74	2.99	0.33	5.00	0.19	-0.49

All energy values are in eV; σ is in eV^{-1}

Molecular electrostatic potential

The mapping of molecular electrostatic potential (ESP) can allow an observation of the regions of high and low electron density in an organic corrosion inhibitor molecule. This can help determine the possible sites in the inhibitor molecule which are susceptible to undergo adsorption interaction with a metal surface [52, 60, 61]. The ESP mapping of the neutral and protonated Cht-EG are displayed in Fig. 10. The different values of ESP are shown in different colours where the most negative ESP regions are shown in red colour, blue shows the region of the most positive ESP while the green colour shows the regions with zero ESP values [52, 60, 61]. It can be seen that in the neutral inhibitor, the most negative potential (red color) is around the heteroatoms (O and N). Upon protonation at N positions, a deep blue coloured region can be observed around the N atoms showing a deficiency of electrons and the possible centres susceptible for undergoing physical adsorption via electrostatic interaction. These results support the trends observed above in the values of the electrophilicity and the nucleophilicity indices (Table 6).

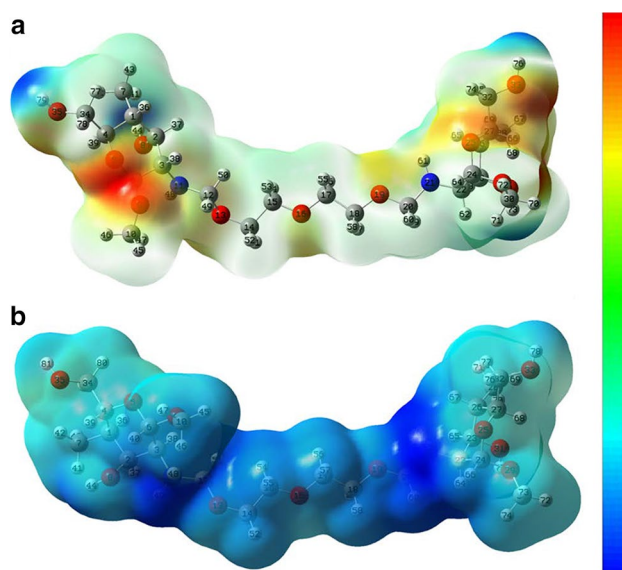


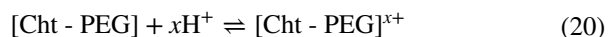
Fig. 10 Molecular electrostatic potential mapping of **a** neutral and **b** protonated Cht-PEG. The bar shows the regions of high (red) and low electron density (blue)



Explanation of adsorption and inhibition

The adsorption of an inhibitor at the metal-solution interface is generally assumed to be the first step in the corrosion inhibition process in an aggressive acid solution. Following mechanism is proposed for the interaction of inhibitor over mild steel surface in the acid solution [62].

1. The inhibitor molecule may get protonated in the acidic medium:



The protonated inhibitor may get adsorbed directly on the surface by forming electrostatic attraction bridges through previously adsorbed acid anion, or, the protonated inhibitor may adsorb via direct electrostatic attraction with the metal surface. The physically adsorbed protonated Cht-PEG molecules may start to compete with the H^+ for electrons over the mild steel surface. The protonated inhibitor, after accepting electrons from the metal surface, then returns to the neutral form [28, 30].

2. The uncharged or neutral inhibitor molecules may then undergo chemical interaction with the metal surface.

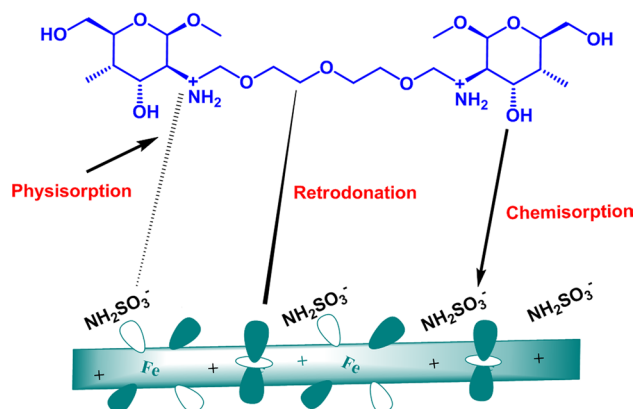


Fig. 11 Schematic of mechanism of adsorption of Cht-PEG on mild steel surface

The presence of heteroatoms (N, S, O, P) in the inhibitor molecule with free lone pair electrons may promote chemical adsorption of the inhibitor over the metal surface.

3. During the corrosion reaction, there can be an accumulation of electrons over the metal surface making it more negatively charged. To relieve this excess negative charge, the electrons from the partially filled d-orbitals of the metal may get transferred to the vacant π anti-bonding orbitals of the inhibitor molecule in a process called retro-donation. This further strengthens the adsorption of inhibitor molecules over the metal surface. A schematic representation of adsorption of inhibitor on mild steel surface is shown in Fig. 11.

A few reports are available on different corrosion inhibitors for sulphamic acid solution for mild steel. A comparison of corrosion inhibition performance of present work with previously tested inhibitors is shown in Table 7. The present work is the first report on the application of Cht-PEG against corrosion of mild steel in sulphamic acid solution. The obtained experimental results in the present work suggest that the Cht-PEG behaves as a promising inhibitor against mild steel corrosion in 1 M sulphamic acid.

Conclusions

In the present study, polyethylene glycol (PEG) cross-linked Chitosan (Cht-PEG) was used as corrosion inhibitor for mild steel in 1 M sulphamic acid solution. Following major conclusions were drawn out of the investigation:

1. Polyethylene glycol (PEG) cross-linked Chitosan (Cht-PEG) exhibited 93.9% inhibition efficiency at 200 mg L^{-1} concentration against the corrosion of mild steel in 1 M sulphamic acid solution.

Table 7 A comparison of the corrosion inhibition behaviour of Cht-PEG with other inhibitors for sulphamic acid

Inhibitor	Metal surface	Sulphamic acid concentration	Inhibition efficiency ($\eta\%$)	References
<i>N</i> -acetylcysteine	Mild steel	5%	97.4	[2]
Cysteine	Mild steel	5%	96.7	[2]
<i>S</i> -benzylcysteine	Mild steel	5%	90.7	[2]
Cystine	Mild steel	5%	93.7	[2]
Methionine	Mild steel	5%	95.9	[2]
Chitosan	Mild steel	1 M	72.38	[11]
Chitosan + KI	Mild steel	1 M	91.68	[11]
Cht-PEG	Mild steel	1 M	93.9	Present work

2. The corrosion inhibition efficiency showed an increase with increase in the concentration of inhibitor. The adsorption of Cht-PEG on the mild steel surface followed Langmuir isotherm and exhibited a mixed mode of adsorption.
3. EIS study showed an increase in the polarization resistance with increase in concentration thereby supporting the formation of a protective film.
4. Polarization study revealed that the tested inhibitor suppresses both anodic and cathodic processes while exhibiting a cathodic predominance.
5. The results of quantum chemical calculations carried out on neutral and protonated inhibitor supported the experimental results and provided evidence for metal-inhibitor interaction.

Acknowledgements Dr. Dheeraj Singh Chauhan gratefully acknowledges King Fahd University of Petroleum and Minerals for Post-doctoral research fellowship. Prof. M.A. Quraishi gratefully acknowledges the financial assistance from DIH Project, IIT (BHU).

Open Access This article is distributed under the terms of the Creative Commons Attribution 4.0 International License (<http://creativecommons.org/licenses/by/4.0/>), which permits unrestricted use, distribution, and reproduction in any medium, provided you give appropriate credit to the original author(s) and the source, provide a link to the Creative Commons license, and indicate if changes were made.

References

1. Motamedi M, Tehrani-Bagha AR, Mahdavian M (2011) A comparative study on the electrochemical behavior of mild steel in sulfamic acid solution in the presence of monomeric and gemini surfactants. *Electrochim Acta* 58:488–496. <https://doi.org/10.1016/j.electacta.2011.09.079>
2. Morad MS (2008) Corrosion inhibition of mild steel in sulfamic acid solution by S-containing amino acids. *J Appl Electrochem* 38:1509–1518. <https://doi.org/10.1007/s10800-008-9595-2>
3. Hermas AA, Morad MS (2008) A comparative study on the corrosion behaviour of 304 austenitic stainless steel in sulfamic and sulfuric acid solutions. *Corros Sci* 50:2710–2717. <https://doi.org/10.1016/j.corsci.2008.06.029>
4. Motamedi M, Tehrani-Bagha AR, Mahdavian M (2013) Effect of aging time on corrosion inhibition of cationic surfactant on mild steel in sulfamic acid cleaning solution. *Corros Sci* 70:46–54. <https://doi.org/10.1016/j.corsci.2013.01.007>
5. Cai L, Fu Q, Shi R, Tang Y, Long Y-T, He X-P, Jin Y, Liu G, Chen G-R, Chen K (2013) ‘Pungent’ copper surface resists acid corrosion in strong HCl solutions. *Ind Eng Chem Res* 53(1):64–69
6. Deng Q, He X-P, Shi H-W, Chen B-Q, Liu G, Tang Y, Long Y-T, Chen G-R, Chen K (2012) Concise CuI-catalyzed azide-alkyne 1, 3-dipolar cycloaddition reaction ligation remarkably enhances the corrosion inhibitive potency of natural amino acids for mild steel in HCl. *Ind Eng Chem Res* 51(21):7160–7169
7. Deng Q, Shi H-W, Ding N-N, Chen B-Q, He X-P, Liu G, Tang Y, Long Y-T, Chen G-R (2012) Novel triazolyl bis-amino acid derivatives readily synthesized via click chemistry as potential corrosion inhibitors for mild steel in HCl. *Corros Sci* 57:220–227
8. Deng Q, Ding N-N, Wei X-L, Cai L, He X-P, Long Y-T, Chen G-R, Chen K (2012) Identification of diverse 1, 2, 3-triazole-connected benzyl glycoside-serine/threonine conjugates as potent corrosion inhibitors for mild steel in HCl. *Corros Sci* 64:64–73
9. Singh P, Ebenso EE, Olasunkanmi LO, Obot IB, Quraishi MA (2016) Electrochemical, theoretical, and surface morphological studies of corrosion inhibition effect of green naphthridine derivatives on mild steel in hydrochloric acid. *J Phys Chem C* 120:3408–3419. <https://doi.org/10.1021/acs.jpcc.5b11901>
10. Verma C, Olasunkanmi LO, Ebenso EE, Quraishi MA, Obot IB (2016) Adsorption behavior of glucosamine-based, pyrimidine-fused heterocycles as green corrosion inhibitors for mild steel: experimental and theoretical studies. *J Phys Chem C* 120:11598–11611. <https://doi.org/10.1021/acs.jpcc.6b04429>
11. Ashassi-Sorkhabi H, Ghalebsaz-Jeddi N (2005) Inhibition effect of polyethylene glycol on the corrosion of carbon steel in sulphuric acid. *Mater Chem Phys* 92:480–486. <https://doi.org/10.1016/j.matchemphys.2005.01.059>
12. El-Haddad MN (2013) Chitosan as a green inhibitor for copper corrosion in acidic medium. *Int J Biol Macromol* 55:142–149. <https://doi.org/10.1016/j.ijbiomac.2012.12.044>
13. Umoren SA, Banera MJ, Alonso-Garcia T, Gervasi CA, Mirífico MV (2013) Inhibition of mild steel corrosion in HCl solution using chitosan. *Cellulose* 20:2529–2545. <https://doi.org/10.1007/s10570-013-0021-5>
14. Umoren SA, Eduok UM (2016) Application of carbohydrate polymers as corrosion inhibitors for metal substrates in different media: a review. *Carbohydr Polym* 140:314–341. <https://doi.org/10.1016/j.carbpol.2015.12.038>
15. Gupta NK, Joshi PG, Srivastava V, Quraishi MA (2017) Chitosan: a macromolecule as green corrosion inhibitor for mild steel in sulfamic acid useful for sugar industry. *Int J Biol Macromol*
16. Mobin M, Rizvi M (2017) Polysaccharide from *Plantago* as a green corrosion inhibitor for carbon steel in 1 M HCl solution. *Carbohydr Polym* 160:172–183
17. Umoren SA, Ogbobe O, Okafor PC, Ebenso EE (2007) Polyethylene glycol and polyvinyl alcohol as corrosion inhibitors for aluminium in acidic medium. *J Appl Polym Sci* 105:3363–3370
18. Umoren SA, Obot IB, Madhankumar A, Gasem ZM (2015) Performance evaluation of pectin as ecofriendly corrosion inhibitor for X60 pipeline steel in acid medium: experimental and theoretical approaches. *Carbohydr Polym* 124:280–291
19. Hassani Najafabadi A, Abdouss M, Faghihi S (2014) Synthesis and evaluation of PEG-O-chitosan nanoparticles for delivery of poor water soluble drugs: Ibuprofen. *Mater Sci Eng C* 41:91–99. <https://doi.org/10.1016/j.msec.2014.04.035>
20. Zhang XG, Teng DY, Wu ZM, Wang X, Wang Z, Yu DM, Li CX (2008) PEG-grafted chitosan nanoparticles as an injectable carrier for sustained protein release. *J Mater Sci Mater Med* 19:3525–3533. <https://doi.org/10.1007/s10856-008-3500-8>
21. Bhattarai N, Ramay HR, Gunn J, Matsen FA, Zhang M (2005) PEG-grafted chitosan as an injectable thermosensitive hydrogel for sustained protein release. *J Control Release* 103:609–624
22. Chauhan DS, Ansari KR, Sorour AA, Quraishi MA, Lgaz H, Salghi R (2018) Thiosemicarbazide and thiocarbonylhydrazide functionalized chitosan as ecofriendly corrosion inhibitors for carbon steel in hydrochloric acid solution. *Int J Biol Macromol* 107:1747–1757
23. Haque J, Srivastava V, Chauhan DS, Lgaz H, Quraishi MA (2018) Microwave-induced synthesis of chitosan Schiff bases and their application as novel and green corrosion inhibitors: experimental and theoretical approach. *ACS Omega* 3(5):5654–5668
24. Prakash N, Vandan SA (2016) Biodegradable polymer based ternary blends for removal of trace metals from simulated industrial wastewater. *Int J Biol Macromol* 83:198–208



25. Kulkarni AR, Hukkeri VI, Sung H, Liang H (2005) A novel method for the synthesis of the PEG-crosslinked Chitosan with a pH-independent swelling behavior. *Macromol Biosci* 5:925–928
26. Ansari KR, Quraishi MA, Singh A, Ramkumar S, Obote IB (2016) Corrosion inhibition of N80 steel in 15% HCl by pyrazolone derivatives: electrochemical, surface and quantum chemical studies. *RSC Adv* 6:24130–24141. <https://doi.org/10.1039/C5RA25441H>
27. ASTM International (1999) Standard practice for preparing, cleaning, and evaluating corrosion test. Significance 90:1–9. <https://doi.org/10.1520/G0001-03R11.2>
28. Baboian R, SWD Jr, Hack HP, Hibner EL, Scully JR (2009) Corrosion tests and standards: application and interpretation, 2nd edn, pp 1–886. <https://doi.org/10.1520/mnl20-2nd-eb>
29. Ansari KR, Quraishi MA, Singh A (2015) Isatin derivatives as a non-toxic corrosion inhibitor for mild steel in 20% H₂SO₄. *Corros Sci* 95:62–70. <https://doi.org/10.1016/j.corsci.2015.02.010>
30. Ansari KR, Quraishi MA, Singh A (2015) Corrosion inhibition of mild steel in hydrochloric acid by some pyridine derivatives: an experimental and quantum chemical study. *J Ind Eng Chem* 25:89–98. <https://doi.org/10.1016/j.jiec.2014.10.017>
31. Ansari KR, Quraishi MA, Singh A (2014) Schiff's base of pyridyl substituted triazoles as new and effective corrosion inhibitors for mild steel in hydrochloric acid solution. *Corros Sci* 79:5–15. <https://doi.org/10.1016/j.corsci.2013.10.009>
32. Yadav DK, Chauhan DS, Ahamad I, Quraishi MA (2013) Electrochemical behavior of steel/acid interface: adsorption and inhibition effect of oligomeric aniline. *RSC Adv* 3:632–646. <https://doi.org/10.1039/C2RA21697C>
33. 1988-038 PRA Becke-DFT.pdf, (n.d.)
34. Lee C, Yang W, Parr RG (1988) Development of the Colle-Salvetti correlation-energy formula into a functional of the electron density. *Phys Rev B* 37:785–789. <https://doi.org/10.1103/PhysRevB.37.785>
35. Frisch M, Trucks GW, Schlegel HB, Scuseria GE, Robb MA, Cheeseman JR, Scalmani G, Barone V, Mennucci B, Petersson GA (2009) Gaussian 09, revision a. 02, gaussian, Inc., Wallingford, CT. 200
36. Yadav DK, Maiti B, Quraishi M (2010) Electrochemical and quantum chemical studies of 3, 4-dihydropyrimidin-2 (1H)-ones as corrosion inhibitors for mild steel in hydrochloric acid solution. *Corros Sci* 52(11):3586–3598
37. Yadav DK, Quraishi M, Maiti B (2012) Inhibition effect of some benzylidenes on mild steel in 1 M HCl: an experimental and theoretical correlation. *Corros Sci* 55:254–266
38. Khadiri A, Saddik R, Bekkouche K, Aouniti A, Hammouti B, Benchat N, Bouachrine M, Solmaz R (2016) Gravimetric, electrochemical and quantum chemical studies of some pyridazine derivatives as corrosion inhibitors for mild steel in 1 M HCl solution. *J Taiwan Inst Chem Eng* 58:552–564. <https://doi.org/10.1016/j.jtice.2015.06.031>
39. El-Hajjaji F, Messali M, Aljuhani A, Aouad MR, Hammouti B, Belghiti ME, Chauhan DS, Quraishi MA (2018) Pyridazinium-based ionic liquids as novel and green corrosion inhibitors of carbon steel in acid medium: electrochemical and molecular dynamics simulation studies. *J Mol Liq* 249:997–1008
40. Solmaz R, Kardaş G, Çulha M, Yazici B, Erbil M (2008) Investigation of adsorption and inhibitive effect of 2-mercaptothiazoline on corrosion of mild steel in hydrochloric acid media. *Electrochim Acta* 53:5941–5952. <https://doi.org/10.1016/j.electacta.2008.03.055>
41. Popova A, Christov M (2006) Evaluation of impedance measurements on mild steel corrosion in acid media in the presence of heterocyclic compounds. *Corros Sci* 48:3208–3221. <https://doi.org/10.1016/j.corsci.2005.11.001>
42. Singh P, Chauhan DS, Srivastava K, Srivastava V, Quraishi MA (2017) Expired atorvastatin drug as corrosion inhibitor for mild steel in hydrochloric acid solution. *Int J Ind Chem* 8:363–372
43. Özcan M, Dehri I, Erbil M (2004) Organic sulphur-containing compounds as corrosion inhibitors for mild steel in acidic media: correlation between inhibition efficiency and chemical structure. *Appl Surf Sci* 236:155–164
44. Ansari KR, Quraishi MA (2014) Bis-Schiff bases of isatin as new and environmentally benign corrosion inhibitor for mild steel. *J Ind Eng Chem* 20:2819–2829. <https://doi.org/10.1016/j.jiec.2013.11.014>
45. Muralisankar M, Sreedharan R, Sujith S, Bhuvanesh NSP, Sreekanth A (2017) *N*(1)-pentyl isatin-*N*(4)-methyl-*N*(4)-phenyl thiosemicarbazone (PITSc) as a corrosion inhibitor on mild steel in HCl. *J Alloys Compd* 695:171–182. <https://doi.org/10.1016/j.jallcom.2016.10.173>
46. Chong AL, Mardel JI, MacFarlane DR, Forsyth M, Somers AE (2016) Synergistic corrosion inhibition of mild steel in aqueous chloride solutions by an imidazolium carboxylate salt. *ACS Sustain Chem Eng* 4:1746–1755. <https://doi.org/10.1021/acsschemeng.5b01725>
47. Lalitha A, Ramesh S, Rajeswari S (2005) Surface protection of copper in acid medium by azoles and surfactants. *Electrochim Acta* 51:47–55. <https://doi.org/10.1016/j.electacta.2005.04.003>
48. Bahrami MJ, Hosseini SMA, Pilvar P (2010) Experimental and theoretical investigation of organic compounds as inhibitors for mild steel corrosion in sulfuric acid medium. *Corros Sci* 52:2793–2803. <https://doi.org/10.1016/j.corsci.2010.04.024>
49. Geerlings P, De Proft F, Langenaeker W (2010) Conceptual density functional theory. *Chem Rev* 9:1793–1873. <https://doi.org/10.1021/cr990029p>
50. Gece G (2008) The use of quantum chemical methods in corrosion inhibitor studies. *Corros Sci* 50:2981–2992. <https://doi.org/10.1016/j.corsci.2008.08.043>
51. Obot IB, Macdonald DD, Gasem ZM (2015) Density functional theory (DFT) as a powerful tool for designing new organic corrosion inhibitors: Part I: an overview. *Corros Sci* 99:1–30. <https://doi.org/10.1016/j.corsci.2015.01.037>
52. Dohare P, Chauhan D, Sorour A, Quraishi M (2017) DFT and experimental studies on the inhibition potentials of expired Tramadol drug on mild steel corrosion in hydrochloric acid. *Mater Discov* 9:30–41
53. Ansari K, Quraishi M, Singh A, Ramkumar S, Obote IB (2016) Corrosion inhibition of N80 steel in 15% HCl by pyrazolone derivatives: electrochemical, surface and quantum chemical studies. *RSC Adv* 6(29):24130–24141
54. Kaya S, Guo L, Kaya C, Tüzün B, Obot I, Touir R, Islam N (2016) Quantum chemical and molecular dynamic simulation studies for the prediction of inhibition efficiencies of some piperidine derivatives on the corrosion of iron. *J Taiwan Inst Chem Eng* 65:522–529
55. Obot IB, Ebenso EE, Kabanda MM (2013) Metronidazole as environmentally safe corrosion inhibitor for mild steel in 0.5 M HCl: experimental and theoretical investigation. *J Environ Chem Eng* 1(3):431–439
56. Chauhan DS, Ansari K, Sorour A, Quraishi M, Lgaz H, Salghi R (2017) Thiosemicarbazide and thiocarbonylhydrazide functionalized chitosan as ecofriendly corrosion inhibitors for carbon steel in hydrochloric acid solution. *Int J Biol Macromol*
57. Dohare P, Chauhan DS, Hammouti B, Quraishi MA (2017) Experimental and DFT investigation on the corrosion inhibition behavior of expired drug lumerax on mild steel in hydrochloric acid anal. *Bioanal Electrochem* 9:762
58. Geerlings P, De Proft F, Langenaeker W (2003) Conceptual density functional theory. *Chem Rev* 103(5):1793–1874

59. Obot IB, Macdonald DD, Gasem ZM (2015) Density functional theory (DFT) as a powerful tool for designing new organic corrosion inhibitors. Part 1: an overview. *Corros. Sci.* 99:1–30
60. Haque J, Ansari K, Srivastava V, Quraishi M, Obot I (2017) Pyrimidine derivatives as novel acidizing corrosion inhibitors for N80 steel useful for petroleum industry: a combined experimental and theoretical approach. *J Ind Eng Chem* 49:176–188
61. Haque J, Srivastava V, Verma C, Quraishi M (2017) Experimental and quantum chemical analysis of 2-amino-3-((4-((S)-2-amino-2-carboxyethyl)-1H-imidazol-2-yl) thio) propionic acid as new and green corrosion inhibitor for mild steel in 1 M hydrochloric acid solution. *J Mol Liq* 225:848–855
62. Banerjee G, Malhotra SN (1992) Contribution to adsorption of aromatic amines on mild steel surface from HCl solutions by impedance, UV, and Raman spectroscopy. *Corrosion* 48:10–15. <https://doi.org/10.5006/1.3315912>

Publisher's Note Springer Nature remains neutral with regard to jurisdictional claims in published maps and institutional affiliations.

Affiliations

D. S. Chauhan¹ · V. Srivastava² · P. G. Joshi² · M. A. Quraishi¹

✉ D. S. Chauhan
dheeraj.chauhan@kfupm.edu.sa

✉ M. A. Quraishi
mumtaz.quraishi@kfupm.edu.sa

¹ Center of Research Excellence in Corrosion, Research Institute, King Fahd University of Petroleum and Minerals, Dhahran 31261, Saudi Arabia

² Department of Chemistry, Indian Institute of Technology (Banaras Hindu University), Varanasi 221005, India

